AIMS Energy, 14(1): 235–258.
DOI: 10.3934/energy.2026010
Received: 12 December 2025
Revised: 03 February 2026
Accepted: 04 February 2026
Published: 27 February 2026

https://www.aimspress.com/journal/energy

Research article

Robust optimization algorithm for an uncertain EV-integrated microgrid under hybrid scenarios

Guanglin Song[1], Pengyuan Zheng[1,*], Chen Wei[1], Jiabin Xue[1] and Dong Wang[2]

[1] Faculty of Artificial Intelligence, Shanghai University of Electric Power, Shanghai 200090, China
[2] NARI Group (State Grid Electric Power Research Institute), Nanjing 211000, China

* **Correspondence:** Email: pyzheng@shiep.edu.cn; Tel: +8618117562032.

Abstract: For an uncertain microgrid with integrated electric vehicles (EVs), a distributionally robust scheduling algorithm is proposed. First, Monte Carlo simulation is adopted to generate the uncertain region of charging/discharging scenarios for EVs, and a hybrid scenario set for renewable energy and normal load is generated via FCM clustering. In the day-ahead scheduling stage, with the feasibility of the hybrid scenario set and its probability-weighted performance index of the economic cost as the objective function, the optimal power output of the microgrid equipment is calculated to achieve optimal performance of hybrid scenarios by using the column-and-constraint generation algorithm. Subsequently, a robustness test is conducted to ensure the feasibility of the day-ahead optimal solution for any scenario. In the intraday scheduling stage, real-time data on renewable generation, normal load, and electric vehicle are utilized to optimize power adjustment of the day-ahead solution. Results show that the proposed method improves the economic performance of the microgrid system. Simulation cases verify the effectiveness of the proposed method.

Keywords: microgrid; electric vehicle; typical scenarios; extreme scenarios; hybrid scenarios; robust economic dispatch

1. Introduction

Microgrids are an important way to implement a large-scale application of distributed power supply. This new energy management mode realizes energy self-sufficiency and improves energy utilization, integrating distributed power supply, energy storage system, load, and its control

components to form a complete, efficient, and adjustable minigrid. In order to ensure the economic and reliable operation of the microgrid as well as the users' demand, the equipment power output needs to be optimally configured to achieve the interaction between the microgrid and the larger grid. In recent years, with the rapid development of electric vehicles (EVs), large-scale EV connecting into microgrids has increased the load, peak-to-valley difference, and volatility, which in turn leads to a degradation of power quality [1–3]. The technical development of vehicles to microgrids [4] will use EVs as loads or energy storage devices, reducing consumers' electricity costs and ensuring the safe and stable operation of the grid through rational planning. Therefore, it is of great theoretical value and practical significance to consider the uncertainties of new energy, load, and EV (charging and discharging) so as to design a robust optimization for microgrids connected to EVs.

With the incorporation of EVs into optimal microgrid scheduling, researchers have developed deterministic microgrid optimization and uncertain microgrid optimization. Taking EV demand response and interruptible loads into account, Reference [5] constructed a deterministic optimal scheduling framework for islanded microgrid systems with the objective of minimizing system operating costs; Reference [6] leveraged the flexibility of EVs to mitigate the intermittency of renewable energy, establishing a deterministic optimization model that coordinates the control of EV charging/discharging (V2G), energy storage systems, and conventional generators to achieve maximum on-site consumption of renewable energy and minimize operational costs; Reference [7] investigated cross-microgrid energy transactions involving EVs within multi-microgrid systems. A two-layer deterministic optimization model was constructed, where the upper layer represents the microgrid alliance coordination layer, optimizing transaction prices and power flows between microgrids, and the lower layer constitutes the autonomous microgrid layer, where internal resources (including EVs) are scheduled based on the upper-layer electricity prices. Other works [5–7] have ignored the uncertainty of new energy sources, loads, and EV charging and discharging power, resulting in prediction errors and conservatism in scheduling inaccuracies.

In microgrids, there are uncertainties, including interval/box sets, polyhedral uncertainty sets, and ellipsoid/covariance sets. Reference [8] optimized system performance under worst-case scenarios to ensure system robustness based on interval box sets. Reference [9] employed convex hull uncertainty sets to identify and remove outliers from historical data using graph neural networks. It constructed convex hulls based on renewable energy sources (RES) unit pairings, enabling flexible adjustment of conservatism while maintaining computational tractability. Reference [10] utilized ellipsoid/covariance sets to significantly reduce vertex counts while approximating convex hull volumes, thereby balancing robustness and computational efficiency in planning problems.

Uncertain optimization for microgrid connecting to EVs [11] has focused on stochastic optimization [12,13] and robust optimization [14–17]. Reference [12] employed an adaptive stochastic optimization framework to address solar microgrid design and scheduling challenges. It simultaneously proposed a two-stage mixed-integer model for the optimal layout and planning of distributed generation units and energy storage system units. Reference [13] addressed the challenge of resolving grid imbalance characteristics coupled with the randomness of renewable energy, electricity prices, and electric vehicle demand, by proposing a stochastic multi-objective optimization model suitable for grid-connected unbalanced microgrids. The model aimed to minimize both total operating costs and voltage deviation. Reference [14] proposed a two-stage low-carbon robust optimization scheduling model that accounts for EVs, distributed generation, and load uncertainty. This model optimizes scheduling schemes for minimum operating costs under worst-case scenarios

while conducting a detailed analysis of microgrid operating costs under different EV charging modes and the impact of carbon trading mechanisms. Reference [15] proposed a cluster optimal scheduling method for EV clusters with uncertainty in the participation of EV users in demand response. Reference [16] improved a linear decision rule-based microgrid-adjustable robust operation model to reduce the solution conservatism in dealing with renewable energy uncertainty.

For microgrids with V2G-capable EVs, Reference [17] established a two-stage robust optimization framework with a min-max-min structure. Within this framework, both unordered charging and ordered charging/discharging models were developed by using a C&CG algorithm. All of the above studies focused on the worst-case scenarios and constructed robust optimization models to achieve optimal economic performance for such scenarios, without taking into account the performance of other scenarios. Since a worst-case scenario usually has a very small probability of occurring, the above strategy often shows great conservativeness, sacrificing economic performance; this needs further improvement.

To address the uncertainties in new energy sources, normal loads, and the charging and discharging power of EVs, this paper adopts a data-driven approach to generate multiple scenarios including typical scenarios, extreme scenarios, and predictive scenarios. These scenarios are then integrated into a hybrid set to enhance coverage. Based on the hybrid set, a robust optimization method is proposed to optimize the power output of each generation unit and the charging/discharging power of EVs. By optimizing the performance of a hybrid scenario set, the model generates a day-ahead optimal solution that better matches the probable intraday scenarios. The day-ahead optimal solution is passed to the intraday dispatch phase. This approach reduces the adjustment cost of real-time operations, thereby enhancing the overall economic performance of the EV-integrated microgrid system.

The hybrid scenario set integrates typical, extreme, and forecasted scenarios, providing comprehensive coverage. This produces a day-ahead schedule better aligned with actual intraday operations, enhancing economic performance. In contrast, standard distributionally robust optimization focuses on worst-case optimization, often reducing adaptability and economic efficiency when real conditions deviate. Thus, the proposed method offers a structural approach superior to standard distributionally robust optimization. Unlike standard stochastic programming, which requires exact probability distributions, the proposed method uses only historical data, enhancing practicality. It solves the complex semi-infinite optimization via a two-stage game framework. This decomposes the problem for parallel processing and establishes an iterative cycle between data-driven optimization on a hybrid scenario set and robustness verification. This interactive mechanism ensures reliable constraint satisfaction and converges toward a globally optimal solution, fundamentally differentiating it from standard stochastic programming with robust constraints. This approach demonstrates greater universality in practical applications.

2. Microgrid configuration and mathematical modeling

2.1. Basic structure of a microgrid

The grid-connected microgrid system consists of components such as photovoltaic (PV) generation, distributed controllable generation (e.g., diesel generators), energy storage systems, normal loads, demand response loads, and EVs. The specific structure is shown in Figure 1.

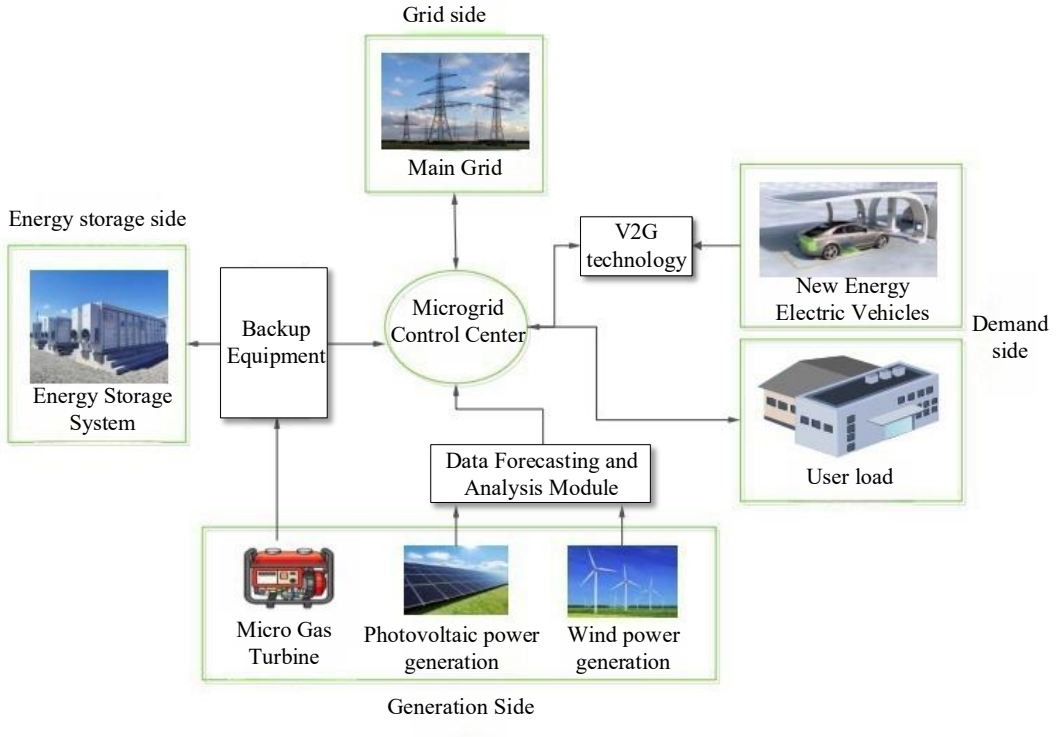

Figure 1. Schematic diagram of a microgrid structure.

2.2. Modeling EV orderly charging and discharging behavior

It is assumed that all EVs connected to the microgrid are private vehicles, and their travelling conforms to a certain regularity. For the battery configuration, the vehicle lithium battery is chosen to have a capacity of 30 kw, an average power consumption of 0.2 kw/h, and a charging power 0.9 kw.

2.2.1. Probability distribution of daily mileage travelled

According to statistics regarding the characteristics of private EV travel, the daily mileage of private vehicles approximately follows a lognormal distribution, and the end time of driving obeys normal distribution. This study assumes that vehicle owners start charging immediately upon trip completion; therefore, the charging start time is also modeled with a normal distribution. The behavior of EVs is modeled based on traveling patterns and habits of conventional private cars [18]. The expression of the probability density function obeyed by the daily travelling mileage is as follows:

$$f_D(x) = \frac{1}{x\delta_D\sqrt{2\pi}} \exp[-\frac{(\ln x - \mu_D)^2}{2\delta_D{}^2}] \tag{1}$$

where $\mu_D = 3.20$; $\delta_D = 0.88$, and the probability density curve for the daily mileage of an EV can be plotted, as shown in Figure 2.

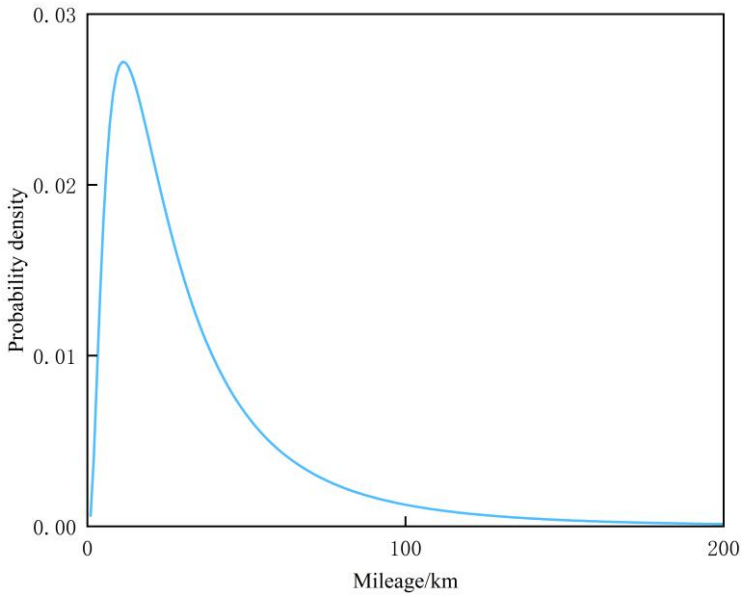

Figure 2. Daily mileage probability distribution curve of EVs.

The EV return time obeys a normal distribution, and its probability density function can be expressed as follows:

$$f_1(x)=\begin{cases}\dfrac{1}{\sigma_t\sqrt{2\pi}}\exp\left[-\dfrac{(x-\mu_t)^2}{2\sigma_t^2}\right], \mu_t-12<x<24\\ \dfrac{1}{\sigma_t\sqrt{2\pi}}\exp\left[-\dfrac{(x-(\mu_t-24))^2}{2\sigma_t^2}\right], 0<x<\mu_t-12\end{cases} \tag{2}$$

where $\mu_s=17.47;\ \delta_s=3.41$ is chosen.

2.2.2. Modeling orderly charging and discharging of EVs

According to the characteristics of orderly charging and discharging, EVs will be controlled to discharge during peak load periods and charge during low load periods. The requirements for charging and discharging are as follows:

(1) From 8:00 to 17:00, some EVs leave the microgrid due to users' workday. The remaining EVs will stay in the microgrid park, subject to the microgrid's economic dispatching.

(2) From 18:00 to 23:00, EV users return home from work, and the microgrid enters its peak load period. To mitigate this, the microgrid schedules EVs to discharge, thereby alleviating the load pressure on the microgrid system. If $SOC < 0.3$, EVs are required to stop discharging to maintain battery life.

(3) From 24:00 to 7:00, the microgrid system enters a period of low load demand and relatively low electricity prices. Therefore, the microgrid schedules EVs for charging.

The latest charging and discharging time for EVs can be expressed by the following equation:

$$T_{dis}^{\max} = \frac{\Delta SOC \cdot C_{EV}}{P_{dis}} - \frac{SW}{100 P_{dis}} \tag{3}$$

where SOC is the deviation value from maximum capacity for the state of charge, W is the power consumption per 100 km, and P_{dis} is the discharge power. The daily mileage S can be calculated by using Eq (1).

Adopting the Monte Carlo method, the fitting curve of EV charging and discharging power is obtained for the EV statistics of the microgrid, as shown in Figure 3.

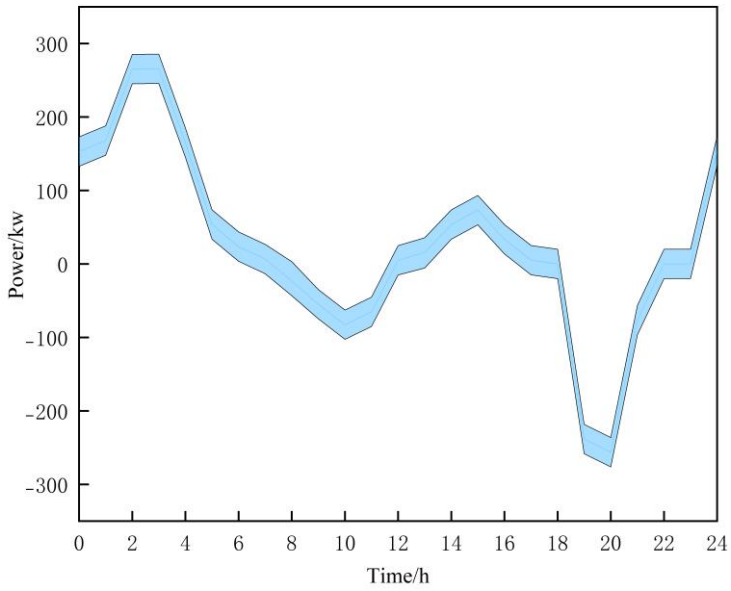

Figure 3. Electric vehicle charging and discharging power curve.

2.3. Mathematical modeling of microgrids

2.3.1 Micro gas turbine

The micro gas turbine is chosen as the core distributed generation unit, and key constraints and costs involved are as follows:

Generation power and climbing rate constraints are described as follows:

$$\Delta P_{DG}^{\min} \le P_{DG}(t) - P_{DG}(t-1) \le \Delta P_{DG}^{\max} \tag{4}$$

$$P_{DG}^{\min} \le P_{DG}(t) \le P_{DG}^{\max} \tag{5}$$

where $P_{DG}(t)$ denotes the output power of the micro gas turbine at time t, $P_{DG}^{\max} / P_{DG}^{\min}$ are used to represent its maximum and minimum output power, respectively, and $\Delta P_{DG}^{\max} / \Delta P_{DG}^{\min}$ denote its maximum and minimum climbing rate, respectively.

The cost function of the micro gas turbine is:

$$C_{DG}(t) = [K_{DG}^{r} + K_{DG}^{m}]P_{DG}(t)\Delta t \tag{6}$$

where K_{DG}^{r} indicates the operation and maintenance cost coefficient of the micro gas turbine, K_{DG}^{m} indicates its fuel cost coefficient, and Δt indicates the sample time interval.

2.3.2 Renewable energy

Renewable energy sources include photovoltaic and wind generation, which are usually derived from natural processes. Without loss of generality, photovoltaic (PV) power generation is selected to represent renewable energy and is denoted as $P_{pv}(t)$ in this paper.

2.3.3 Energy storage unit

The energy storage unit can effectively reduce the peak-valley gap and improve the economy of the microgrid. The dynamic equation of charging and discharging is described as follows:

$$E_S(t) = E_S(0) + \eta\sum_{t=1}^{N_T}[P_S^{ch}(t)\Delta t] - \frac{1}{\eta}\sum_{t=1}^{N_T}[P_S^{dis}(t)\Delta t] \tag{7}$$

where $P_S^{ch}(t)$ / $P_S^{dis}(t)$ are the charging and discharging power of the energy storage unit at time t ,respectively; η represents the charging and discharging efficiency; $E_S(t)$ denotes the state of charge of the energy storage unit; and N_T is the scheduling period.

The following constraints of energy storage unit also need to be satisfied:

$$E_S^{\min} \le E_S(t) \le E_S^{\max} \tag{8}$$

$$0 \le P_S^{ch} \le \delta_S(t)P_S^{\max} \tag{9}$$

$$0 \le P_S^{dis}(t) \le [1-\delta_S(t)]P_S^{\max} \tag{10}$$

where $E_S^{\min}$ / $E_S^{\max}$ are the minimum and maximum values of the state of charge allowed for the energy storage unit, respectively; $P_S^{\max}(t)$ is the maximum charge/discharge power allowed for energy storage; and $\delta_S(t)$ is a binary variable that represents the status flag of charging and discharging.

In order to make the cyclic scheduling of the energy storage unit more convenient, the following constraint is also imposed:

$$E_S(0) = E_S(N_T) \tag{11}$$

The cost function of the energy storage unit is formulated as follows:

$$C_S(t) = K_S[\eta P_S^{ch}(t) + \frac{1}{\eta} P_S^{dis}(t)]\Delta t \tag{12}$$

where K_S denotes the maintenance cost coefficient of the energy storage unit.

2.3.4 Demand response load

In this paper, the microgrid load includes normal load and demand response load. As for the demand response load, the constraints are described as follows:

$$\sum_{t=1}^{N_T} P_{DR}(t) = D_{DR} \tag{13}$$

$$P_{DR}^{\min} \le P_{DR}(t) \le P_{DR}^{\max} \tag{14}$$

where $P_{DR}(t)$ denotes the actual electricity power of the demand response load at time t; D_{DR} denotes the total load amount over the overall scheduling period; and $P_{DR}^{\min} / P_{DR}^{\max}$ are the minimum/maximum power consumption of the demand response load, respectively.

The demand response load can be flexibly regulated with the following adjustment cost:

$$C_{DR}(t) = K_{DR} \left| P_{DR}(t) - P_{DR}^{*}(t) \right| \Delta t \tag{15}$$

where $P_{DR}^{*}(t)$ denotes the expected electricity plan of the demand response load at time t, and K_{DR} indicates its adjusted compensation cost coefficient. By introduction of auxiliary variables P_{DR1} / P_{DR2}, Eq (15) can be linearized as follows:

$$C_{DR}(t) = D_{DR}[P_{DR1}(t) + P_{DR2}(t)]\Delta t \tag{16}$$

$$P_{DR}(t) - P_{DR}^{*} + P_{DR1}(t) - P_{DR2}(t) = 0 \tag{17}$$

$$P_{DR1}(t) \ge 0, P_{DR2}(t) \ge 0 \tag{18}$$

2.3.5 Power interaction of a large grid

The microgrid interacts with the power from the main grid to deliver power to the main grid when there is an excess of renewable energy generation, and to obtain power from the main grid when there is a shortage of generation, thereby regulating its power balance. To ensure that the microgrid can operate stably and meet the following constraints:

$$0 \le P_G^{\text{buy}}(t) \le U_M(t) P_G^{\max} \tag{19}$$

$$0 \le P_G^{sell}(t) \le (1 - U_M(t)) P_G^{\max} \tag{20}$$

where $P_G^{buy}(t) / P_G^{sell}$ denote the purchase/sale power, respectively; $U_M(t)$ indicates the status flag of power purchase/sale operation; and $P_G^{\max}$ represents the maximum value of power interaction with the larger grid.

The cost function for interaction with the large grid is formulated as follows:

$$C_G = K_G[P_G^{buy}(t) - P_G^{sell}(t)]\Delta t \tag{21}$$

where $K_G(t)$ represents the day-ahead electricity price of the large grid.

2.3.6 Power balance constraints for microgrid system

The microgrid has to maintain a power balance at every moment during its operation; thus, the following power balance constraints should be satisfied:

$$P_G^{buy}(t) + P_{DG}(t) + P_S^{dis} + P_{PV}(t) + P_{EV}^{dis}(t) = P_G^{sell}(t) + P_S^{ch}(t) + P_{DR}(t) + P_L(t) + P_{EV}^{ch}(t) \tag{22}$$

where $P_{EV}^{ch}(t) / P_{EV}^{dis}(t)$ denote the charging/discharging power of EVs.

2.3.7 The economic cost function of microgrid

The economic cost function of the grid-connected microgrid is formulated as:

$$\min \sum_{t=1}^{N_T} \left[C_{DG}(t) + C_S(t) + C_{DR}(t) + C_G(t) \right] \tag{23}$$

3. Data-driven hybrid scenario sets

For microgrids, the uncertainty of new energy, normal load, and EVs can be described as follows:

$$U := \begin{cases} u = [u_{PV}(t), u_L(t), u_{EV}(t)]^T \in R^{(N_T)\times 3}, t = 1, 2, \cdots, \ N_T \\ u_{PV}(t) \in \left[\hat{u}_{pv}(t) - \Delta u_{pv}^{\max}, \hat{u}_{pv}(t) + \Delta_{pv}^{\max} \right] \\ u_L(t) \in \left[\hat{u}_L(t) - \Delta u_L^{\max}, \hat{u}_L(t) + \Delta_L^{\max} \right] \\ u_{EV}(t) \in \left[\hat{u}_{EV}(t) - \Delta u_{EV}^{\max}, \hat{u}_{EV}(t) + \Delta_{EV}^{\max} \right] \end{cases} \tag{24}$$

where u_{pv}, u_L, and u_{EV} denote the actual power value of photovoltaic power, normal load, and electrical vehicles, respectively; $\hat{u}_{pv}$, $\hat{u}_L$, and $\hat{u}_{EV}$ denote the predicted value of photovoltaic power, normal load, and electrical vehicles, respectively; and $\Delta u_{pv}^{\max}$, $\Delta u_L^{\max}$, and $\Delta u_{EV}^{\max}$ represent the maximum fluctuation range for photovoltaics, normal loads, and EVs, respectively.

Within the uncertainty set, the worst-case scenario usually occurs at its boundaries. Therefore, Eq (24) can be converted into:

$$U^* := \begin{cases} u_j \in \left[u_{PV}, u_L, u_{EV}\right]^T \in R^{(N_T)\times 3} \\ u_j(t) = u_j(t) + \left(\tau_{j,t}^+ - \tau_{j,t}^-\right)\Delta u_j(t) \\ \tau_{j,t}^+, \tau_{j,t}^- \in \{0,1\} \\ \tau_{j,t}^+ + \tau_{j,t}^- \le 1 \\ \sum_{t=1}^{N_T} \tau_{j,t}^+ + \tau_{j,t}^- \le \Gamma_j, j \in \{PV, L, EV\} \end{cases} \tag{25}$$

where $\tau_{j,t}^+, \tau_{j,t}^-$ are the binary variables, and $\Gamma_{pv}, \Gamma_L, \Gamma_{EV}$ denote the time intervals during which the PV/load/EV power can deviate to its boundaries, respectively.

As is well known, robust optimization based on the traditional tube uncertainty sets Eqs (24) and (25) mainly focuses on the performance of worst-case scenarios. The corresponding solution has some conservativeness, and performance will be degraded, especially when real conditions deviate from the worst-case scenarios. To overcome conservativeness, this paper adopts the following clustering method to derive typical scenarios and extreme scenarios with probabilistic distributions from historical data.

3.1. Generation of typical scenarios and probability calculation

Typical scenarios, extreme scenarios, and their probabilities will be generated using the FCM [19] clustering algorithm. For M historical scenarios data, the FCM clustering algorithm is applied to generate N clusters of scenarios U_i^c, $i = 1,2,\ldots,N$, in which the i-th scenario U_i^c encompasses M_i historical scenarios with $\sum_{i=1}^{N} M_i = M$. The center of U_i^c is chosen as its typical scenario $u_i^t, i = 1,2,\ldots,N$ with initial probability $p_i^t = M_i / M$ [20]. The set $U^t = \{u_1^t, u_2^t, \ldots, u_N^t\}$, consisting of typical scenarios, is defined as the typical scenario set.

3.2. Generation of the extreme scenario and its probability

From the i-th scenario cluster U_i^c, choose an extreme scenario that has the smallest affiliation with typical scenarios u_i^t and denote it as $u_i^e (i = 1,2,\cdots,N)$. The initial probability of the extreme scenario is calculated by $P_i^e = 1/M$. In a similar way, N extreme scenarios $u_1^e, u_N^e, \cdots, u_N^e$ can be obtained from N clusters of scenarios.

3.3. Hybrid scenario sets and their probabilities

Placing typical scenarios, the extreme scenario sequence $U^e = \{u_1^e, u_2^e, \ldots, u_N^e\}$, and the predictive

scenario $\hat{u}$ together, the hybrid scenario set $U^h = \left\{u_1^h, u_2^h, \ldots, u_{2N}^h, u_{2N+1}^h\right\}$ is formed, whose elements take the following values:

$$\begin{cases} u_i^h = u_i^t, 1 \le i \le N \\ u_i^h = u_i^e, N+1 \le i \le 2N \\ u_{2N+1}^h = \hat{u} \end{cases} \tag{26}$$

Specifying $u_1^h, u_2^h, \ldots, u_{2N+1}^h$ as the series of clustering centers, historical scenario data are clustered again using the FCM clustering algorithm. For u_i^h ($i = 1,2,\ldots,2N+1$), if K_i historical scenarios are reassigned to it by the FCM clustering algorithm, its probability will be denoted as $p_i^h = K_i / M$. By analogy, the probability $p_1^h, p_2^h, \ldots, p_{2N}^h, p_{2N+1}^h$ can be obtained.

4. Robust optimization algorithm for an uncertain EV-integrated microgrid under hybrid scenarios (HSEV-RO)

4.1. Day-ahead scheduling

In order to better balance the performance of each scenario, this paper designs a robust optimization algorithm based on the performance of hybrid scenario sets, which can be expressed in the following compact form:

$$\min_{x,y} \sum_{m=1}^{2N+1} p_m^h c^T y_m^* \tag{27}$$

$$\begin{aligned} s.t. \quad & Dx + Fy_1^* \ge Gu_1^h - H \\ & Dx + Fy_2^* \ge Gu_2^h - H \\ & \vdots \\ & Dx + Fy_{2N+1}^* \ge Gu_{2N+1}^h - H \end{aligned} \tag{28}$$

$$\forall u \in U^*, \exists y : Fy \ge Gu - Dx - H \tag{29}$$

$$x = (x_1, x_2 \cdots, x_{2N_T})^T \tag{30}$$

$$x_i \in \{0,1\}, \forall i \in (1,2,\cdots,2N_T) \tag{31}$$

$$y_j^* \ge 0, y \ge 0, j \in (1,2,\cdots,2N+1) \tag{32}$$

with the following symbol abbreviations:

$$\begin{cases} x = \left[U_S(t), U_M(t)\right]^T \\ y = \begin{bmatrix} P_{DG}(t), P_S^{ch}(t), P_S^{dis}(t), P_{DR}(t), P_{DR1}(t), P_{DR2}(t) \\ P_G^{buy}(t), P_G^{sell}(t), P_{PV}(t), P_L(t), P_{EV}^{ch}(t), P_{EV}^{dis}(t) \end{bmatrix} \end{cases} \tag{33}$$

where c is the coefficient column vector corresponding to the microgrid cost functions (6), (12), (15), and (21), $p_m^h c^T y_m^*$ indicates the multiplication of their operation costs $c^T y_m^*$ for scenario u_m^h and the corresponding probability p_m; D, G, F, and H denote the coefficient matrix and column vector corresponding to microgrid constraints (4), (5), (7–11), (13), (14), (17–20), respectively. Eq (27) incorporates both the operation cost and probability of the hybrid scenarios. Therefore, it efficiently enhances economics not only for the high probability scenarios but also for extreme cases with low probability.

Equation (29) guarantees the feasibility of microgrid optimization with uncertainty. Even for the worst case, the method can also generate feasible and efficient scheduling schemes, which significantly improves the performance of microgrid operation.

The optimization problem (27) generates the pre-scheduling solution $X^* = [U_s^*(t),\ U_M^*(t)]$. To ensure that this pre-scheduling solution is also feasible for other scenarios in the uncertainty set U^*, robust tests will be designed.

4.2. Robust testing model

By introducing slack variables $r^+ \geq 0$, $r^- \geq 0$ for the power surplus/deficit, the power balance equation is rewritten as follows:

$$P_G^{buy}(t) + P_{DG}(t) + P_S^{dis} + P_{PV}(t) + P_{EV}^{dis} = P_G^{sell}(t) + P_S^{ch}(t) + P_{DR}(t) + P_L(t) + P_{EV}^{ch} + r^+ + r^- \tag{34}$$

The cumulative value of the power gap over the entire scheduling period is defined as follows:

$$R(x) = \max_{u \in U} \min_{y, r_t^+, r_t^-} \sum_{t=1}^{N_T} r_t^+ + r_t^- \tag{35}$$

Based on Eq (35), the optimization problem (27) is transformed as follows:

$$\begin{cases} \min\limits_{x,y} \sum\limits_{m=1}^{2N+1} p_m^h c^T y_m^* \\ s.t. Dx + Fy_1^* \geq Gu_1 - H \\ \vdots \\ Dx + Fy_{2N+1}^* \geq Gu_{2N+1} - H \\ R(x) = 0 \end{cases} \tag{36}$$

where $R(x) = 0$ indicates that the power balance of the microgrid system can be satisfied when PV,

normal load, and electric vehicle charging/discharging power vary within the uncertainty set.

By applying the strong duality theory, the max-min problem in Eq (35) is transformed into a max problem, and the final robust test model is obtained as follows:

$$
\begin{aligned}
R = \max_{\substack{\varphi_t^+,\varphi_t^-,\lambda_t^+,\lambda_t^-,\mu_t^+,\beta_t^+,\\ \pi_t^+,\pi_t^-,\theta_t^+,\theta_t^-,\kappa_t,\varepsilon_t^+,\\ \omega_t^+,\sigma_t,\psi,z_{j,t}^+,z_{j,t}^-,}} \tau_{j,t}^+,\tau_{j,t}^- \sum_{t=1}^{N_T} \Big\{ & -P_{DG}^{\max}\varphi_t^+ + P_{\mathrm{DG}}^{\min}\varphi_t^- + \\
& \left[-E_{\mathrm{S}}^{\max} + E_{\mathrm{S}}(0)\right]\pi_t^+ + \left[E_{\mathrm{S}}^{\min} - E_{\mathrm{S}}(0)\right]\pi_t^- \\
& -U_{\mathrm{S}}^*(t)P_{\mathrm{S}}^{\max}\mu_t^+ + \left[U_{\mathrm{S}}^*(t)-1\right]P_{\mathrm{S}}^{\max}\beta_t^+ \\
& +\mathrm{D}_{DR}\gamma_t - P_{DR}^{\max}\theta_t^+ + P_{DR}^{\min}\theta_t^- + P_{DR}^*(t)\kappa_t \\
& -U_M^*(t)P_{\mathrm{G}}^{\max}\varepsilon_t^+ + \left[U_M^*(t)-1\right]P_{\mathrm{G}}^{\max}\omega_t^+ \Big] \\
& +\lambda_1^+\left[-P_{\mathrm{DG}}(0) - \Delta P_{\mathrm{DG}}^{\max}\right] \\
& +\lambda_1^-\left[P_{\mathrm{DG}}(0) + \Delta P_{\mathrm{DG}}^{\min}\right] + \psi E_{\mathrm{S}}(0) \\
& +\sum_{t=2}^{N_T}\left(-\lambda_t^+\Delta P_{\mathrm{DG}}^{\max} + \lambda_t^-\Delta P_{\mathrm{DG}}^{\min}\right) + \\
& [\hat{u}_{EV}(t) + \hat{u}_{\mathrm{L}}(t) - \hat{u}_{\mathrm{PV}}(t)]\sigma_t + \\
& \Delta u_{EV}(t)\left(z_{EV,t}^+ - z_{EV,t}^-\right) + \Delta u_{\mathrm{L}}(t)\left(z_{\mathrm{L},t}^+ - z_{\mathrm{L},t}^-\right) \\
& -\Delta u_{\mathrm{PV}}(t)\left(z_{\mathrm{PV},t}^+ - \overline{z}_{\mathrm{PV},t}\right)\Big\}
\end{aligned}
\tag{37}
$$

$$
\begin{aligned}
\text{s.t.} \; & -\lambda_t^+ + \lambda_t^- + \lambda_{t+1}^+ - \lambda_{t+1}^- - \varphi_t^+ + \varphi_t^- + \sigma_t \le 0, \forall t \in [1, N_{\mathrm{T}} - 1] \\
& -\mu_t^+ + \mu_t^- - \eta \cdot \Delta t \cdot \pi_t^+ - \sigma_t \le 0, \forall t \in [1, N_{\mathrm{T}} - 1] \\
& \beta_t^+ + \beta_t^- - \frac{1}{\eta} \cdot \Delta t \cdot \pi_t^+ + \sigma_t \le 0, \forall t \in [1, N_{\mathrm{T}} - 1] \\
& -1 \le \sigma_t \le 1, \forall t \in [1, N_{\mathrm{T}}] \\
& \gamma_t - \theta_t^+ + \theta_t^- + \sigma_t \le 0, \forall t \in [1, N_{\mathrm{T}}] \\
& -\varepsilon_t^+ + \varepsilon_t^- + \sigma_t \le 0, \forall t \in [1, N_{\mathrm{T}}] \\
& -\omega_t^+ + \omega_t^- - \sigma_t \le 0, \forall t \in [1, N_{\mathrm{T}}] \\
& -e_t^+ + e_t^- - \alpha_{t+1} + \alpha_t \le 0, \forall t \in [1, N_{\mathrm{T}}] \\
& -\lambda_{N_{\mathrm{T}}}^+ + \lambda_{N_{\mathrm{T}}}^- - \varphi_{N_{\mathrm{T}}}^+ + \varphi_{N_{\mathrm{T}}}^- + \sigma_{N_{\mathrm{T}}} \le 0 \\
& -e_{N_{\mathrm{T}}}^+ + e_{N_{\mathrm{T}}}^- + \alpha_{N_{\mathrm{T}}} + \psi \le 0 \\
& \tau_{j,t}^+, \tau_{j,t}^- \in \{0,1\} \\
& \tau_{j,t}^+ + \tau_{j,t}^- \le 1 \\
& \sum_{t=1}^{N_T} \tau_{j,t}^+ + \tau_{j,t}^- \le \Gamma_j, j \in \{PV, L, EV\}
\end{aligned}
\tag{38}
$$

Remark: The constraints attached to the optimization problem in Eq (27) are derived from Eqs (4), (5), (7–11), (13), (14), (17–20), and (22) by use of the strong duality theory. In Eqs (37) and (38), λ_t^+, λ_t^-, φ_{t}^+, φ_{t}^-, π_t^+, π_t^-, μ_t^+, β_t^+, ψ, γ_t, θ_t^+, θ_t^-, κ_t, ε_t^+, ω_t^+, σ_t are the introduced dual variables, being non-negative and $z_{j,t}^+ = \sigma_t \cdot \tau_{j,t}^+$, $z_{j,t}^- = \sigma_t \cdot \tau_{j,t}^-$, $j \in \{PV, L, EV\}$. Each dual variable

corresponds to its respective formula as follows: λ_t^+, λ_t^- corresponds to formula (4), φ_t^+, φ_t^- corresponds to formula (5), π_t^+, π_t^- corresponds to formula (8), μ_t^+ corresponds to formula (9), β_t^+ corresponds to formula (10), ψ corresponds to formula (11), γ_t corresponds to formula (13), θ_t^+, θ_t^- corresponds to formula (14), κ_t corresponds to formula (17), ε_t^+ corresponds to formula (19), ω_t^+ corresponds to formula (20), and σ_t corresponds to formula (22).

For ease of data citation in the following text, the power output of energy storage unit, electric vehicle, demand response load, and grid interaction obtained in the day-ahead stage are denoted as $P_S^{ch^*}(t)/P_S^{dis^*}(t)$, $P_{EV}^{ch^*}(t)/P_{EV}^{dis^*}(t)$, $P_{DR}^*(t)$, and $P_G^{buy^*}/P_G^{sell^*}$, respectively.

4.3. Intraday scheduling

Considering that the dynamics of energy storage unit (EV battery system) have strong time coupling characteristics, and the demand response load has the total amount over the overall scheduling period, the power output of the energy storage unit, electric vehicle, and demand response load in intraday stage is required to retain the value of $P_S^{ch^*}(t)/P_S^{dis^*}(t)$, $P_{EV}^{ch^*}(t)/P_{EV}^{dis^*}(t)$, and $P_{DR}^*(t)$. Thus, the power output of the micro gas turbine and grid interaction will be adjusted in the intraday stage.

The actual power output of the micro gas turbine, denoted as $\hat{P}_{DG}(t)$, is adjusted by minimizing the following penalty cost:

$$C_{DG}^{adj}(t) = K_{DG}[\hat{P}_{DG}(t) - P_{DG}^*(t)] + C_{DG}^{pen}(t) \tag{39}$$

$$C_{DG}^{pen}(t) = K_{DG}^{add}\max[\hat{P}_{DG}(t) - P_{DG}^*(t), 0] + K_{DG}^{dec}\min[\hat{P}_{DG}(t) - P_{DG}^*(t), 0] \tag{40}$$

where K_{DG} denotes the operation and management cost coefficient, and $K_{DG}^{\text{add}}/K_{DG}^{dec}$ are the penalty coefficients introduced to limit the power adjustment magnitude.

By introducing auxiliary variables $P_{DG1}(t)$, $P_{DG2}(t)$, Eq (40) can be linearized as follows:

$$C_{DG}^{pen}(t) = \left(K_{DG}^{add} + K_{DG}^{dec}\right)\left[\frac{\hat{P}_{DG}(t) - P_{DG}^*(t)}{2}\right] + \left(K_{DG}^{add} - K_{DG}^{dec}\right)\left[\frac{P_{DG1}(t) + P_{DG2}(t)}{2}\right] \tag{41}$$

$$P_{DG}(t) - P_{DG}^*(t) + P_{DG1}(t) - P_{DG2}(t) = 0 \tag{42}$$

$$P_{DG1}(t) \geq 0, P_{DG2}(t) \geq 0 \tag{43}$$

The adjustment cost function for the main grid interaction is formulated as follows:

$$C_G^{adj}(t) = K_G\left\{\left[\hat{P}_G^{buy}(t) - P_G^{buy^*}(t)\right] - \left[\hat{P}_G^{sell}(t) - P_G^{sell^*}(t)\right]\right\} + C_G^{pen}(t) \tag{44}$$

$$C_G^{pen}(t)=\lambda(t)\Big\{K_G^{add}max\Big[\hat{P}_G^{buy}(t)-P_G^{buy^*}(t),0\Big]+K_G^{dec}\min\Big[\hat{P}_G^{buy}(t)-P_G^{buy^*}(t),0\Big]+$$
$$K_G^{add}\max\Big[\hat{P}_G^{sell}(t)-P_G^{sell^*}(t),0\Big]+K_G^{dec}\min\Big[\hat{P}_G^{sell}(t)-P_G^{sell^*}(t),0\Big]\Big\} \tag{45}$$

where $\hat{P}_G^{buy}(t)/\hat{P}_G^{sell}(t)$ denote the actual purchased power and sold power, respectively; K_G represents the adjusted coefficient; and K_G^{add}/K_G^{dec} denote the penalty coefficients for grid interaction.

In a similar way, by introducing the auxiliary variables $P_{G1}^{buy}(t)$, $P_{G2}^{buy}(t)$, $P_{G1}^{sell}(t)$, P_{G2}^{sell}, Eq (45) can be transformed as:

$$C_G^{pen}(t)=K_G\Bigg\{\Big(K_G^{add}+K_G^{dec}\Big)\Bigg[\frac{\hat{P}_G^{buy}(t)-P_G^{buy^*}(t)}{2}\Bigg]+\Big(K_G^{add}-K_G^{dec}\Big)\Bigg[\frac{P_{G1}^{buy}(t)+P_{G2}^{buy}(t)}{2}\Bigg]+$$
$$\Big(K_G^{add}+K_G^{dec}\Big)\Bigg[\frac{\hat{P}_G^{sell}(t)-P_G^{sell^*}(t)}{2}\Bigg]+\Big(K_G^{add}-K_G^{dec}\Big)\Bigg[\frac{P_{G1}^{sell}(t)+P_{G2}^{sell}(t)}{2}\Bigg]\Bigg\} \tag{46}$$

$$\hat{P}_G^{sell}(t)-P_G^{sell^*}(t)+P_{G1}^{sell}(t)-P_{G2}^{sell}(t)=0 \tag{47}$$

$$\hat{P}_G^{buy}(t)-P_G^{buy}*(t)+P_{G1}^{buy}(t)-P_{G2}^{buy}(t)=0 \tag{48}$$

$$P_{G1}^{sell}(t)\geqslant 0,P_{G2}^{sell}(t)\geqslant 0,P_{G1}^{buy}(t)\geqslant 0,P_{G2}^{buy}(t)\geqslant 0 \tag{49}$$

The magnitudes of coefficients K_{DG}^{add} and K_G^{add} are relative, and their values should maintain a reasonable ratio. The relationship between K_{DG}^{dec} and K_G^{dec} is the same.

Consequently, the power balance equation can be reformulated as follows:

$$\hat{P}_G^{buy}(t)+\hat{P}_{DG}(t)+P_S^{dis*}(t)+\hat{P}_{PV}(t)+P_{EV}^{dis*}(t)=\hat{P}_G^{sell}(t)+P_S^{ch*}(t)+P_{DR}^{*}(t)+\hat{P}_L(t)+\hat{P}_{EV}^{ch*}(t) \tag{50}$$

where $\hat{P}_{PV}(t)$ and $\hat{P}_L(t)$ represent the actual power output of PV and normal load, respectively.

In summary, the intraday scheduling problem can be formulated as follows:

$$\min_{\substack{\hat{P}_{DG},P_{DG1},P_{DG2},\hat{P}_G^{buy},P_{G1}^{buy},\\ \hat{P}_{G2}^{buy},\hat{P}_G^{sell},P_{G1}^{sell},P_{G2}^{sell}}}\Big(C_{DG}^{adj}(t)+C_G^{adj}(t)\Big)$$
$$s.t.(4)(5),(19)(20),(42)(43),(47)-(50) \tag{51}$$

4.4. The process of the HSEV-RO algorithm

Day-ahead scheduling stage:

(1) Initialize the number of iterations k = 0, and the system power gap is 0. Generate a collection of hybrid scenarios $U=\{u_1,u_2,\cdots,u_{2N+1}\}$ based on the scenario clustering algorithm.

(2) Solve the pre-scheduling model as follows:

$$\begin{aligned} &\min_{x,y} \sum_{m=1}^{2N+1} p_m^h c^T y_m^* \\ s.t. \quad & Dx + Fy_1^* \geq Gu_1 - H \\ & Dx + Fy_2^* \geq Gu_2 - H \\ & \vdots \\ & Dx + Fy_{2N+1}^* \geq Gu_{2N+1} - H \\ & Dx + Fy_l \geq Gu_l^* - H, \forall 0 \leq l \leq k \end{aligned} \tag{52}$$

and the optimal solution $(x_{k+1}^*,\ y_{1,k+1}^*, y_{2,k+1}^*,\cdots, y_{2N+1,k+1}^*)$ can be obtained.

(3) Execute robust testing in Eq (37) for x_{k+1}^* and calculate the power gap R_{k+1}. If $R_{k+1} \neq 0$, the following constraint is added to the pre-scheduling model (52), and the procedure jumps to step (2).

$$Dx + Fy_{k+1} \geq Gu_{k+1} - H \tag{53}$$

If $R_{k+1} = 0$, it indicates that x_{k+1}^* is a robust feasible solution. Thus, $y^* = \sum_{m=1}^{2N+1} p_m^h y_m^*$ is selected.

Intraday scheduling stage:

(4) Measure the actual power output of PV and normal load $\hat{P}_{PV}(t) / \hat{P}_L(t)$. Solve the optimization problem (51) to obtain $\hat{P}_{\mathrm{DG}}(t)$, $\hat{P}_{\mathrm{G}}^{\mathrm{buy}}(t) / \hat{P}_{\mathrm{G}}^{\mathrm{sell}}(t)$. Then, the optimal intraday solution is comprised of P_{DR}^*, $P_s^{ch^*} / P_s^{dis^*}$, $\hat{P}_{\mathrm{DG}}(t)$, $\hat{P}_{\mathrm{G}}^{\mathrm{buy}}(t) / \hat{P}_{\mathrm{G}}^{\mathrm{sell}}(t)$.

The flowchart is shown in Figure 4.

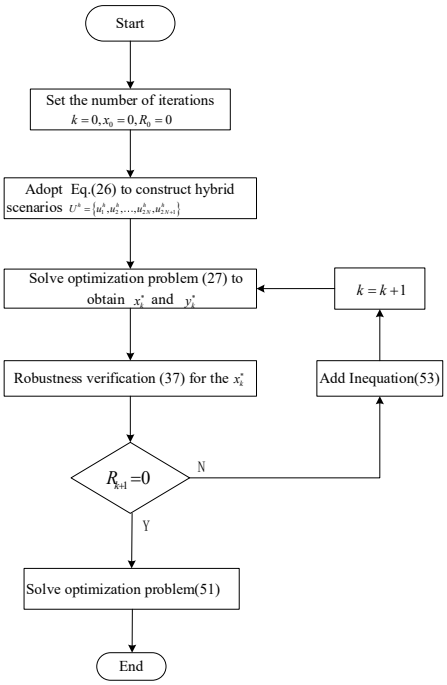

Figure 4. Flowchart of the HSEV-RO algorithm.

5. Simulation results and discussion

To evaluate the effectiveness of the proposed algorithm, the grid-connected microgrid system connecting to EVs shown in Figure 1 was simulated. All simulation calculations were performed on a personal computer equipped with an Intel i5-9600 processor and 16 GB of memory, utilizing the MATLAB R2023a platform and IBM ILOG CPLEX 12.10.0 software.

The relevant parameters of the microgrid are listed in Table 1, and a time-of-use electricity price was adopted and shown in Figure 5. The number of clusters was set to N = 3, and the corresponding hybrid scenarios for the PV, normal load, and EV are shown in Figures 6–8, respectively.

Table 1. Operating parameters of the microgrid.

Unit	Parameters	Numerical value
Micro gas turbine	$P_{DG}^{\min} / P_{DG}^{\max} / kw$	80/800
	$\Delta P_{DG}^{\min} / \Delta P_{DG}^{\max} / kw$	600/600
	$K_{DG}^{r} / K_{DG}^{m} / \left(CNY / \left(kw \cdot h\right)\right)$	0.5/0.15
	$K_{DG}^{add} / K_{DG}^{dec} / \left(CNY / kw \cdot h\right)$	0.5/−0.5
Energy storage	$P_{S}^{\max} / kw$	500
	$E_{S}^{\min} / E_{S}^{\max} / \left(kw \cdot h\right)$	300/1500
	$E_{S}\left(0\right) / \left(kw \cdot h\right)$	1000
	$K_{S} / \left(CNY / \left(kw \cdot h\right)\right)$	0.38
	η	0.95
Demand response load	$D_{DR} / kw \cdot h$	2940
	$P_{DR}^{\min} / P_{DR}^{\max} / kw$	30/200
	$K_{DR} / \left(CNY / \left(kw \cdot h\right)\right)$	0.32
Power interaction	$P_{G}^{\max} / \left(kw \cdot h\right)$	1500
	$K_{G}^{add} / K_{G}^{dec} / \left(CNY / kw \cdot h\right)$	1.0/−0.8

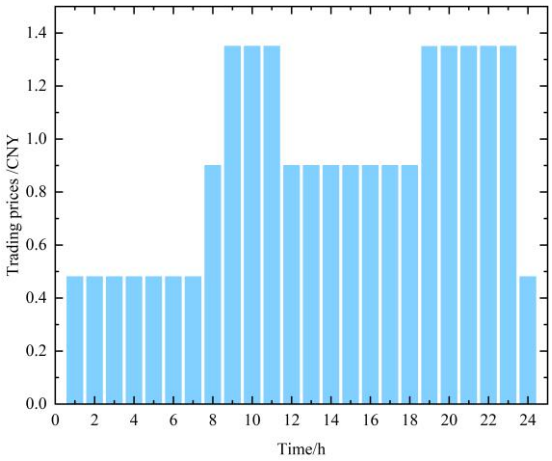

Figure 5. Distribution of electricity trading prices.

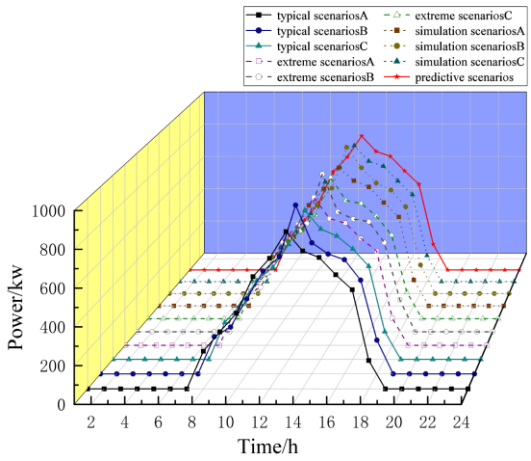

Figure 6. PV power output of the hybrid and simulation scenarios.

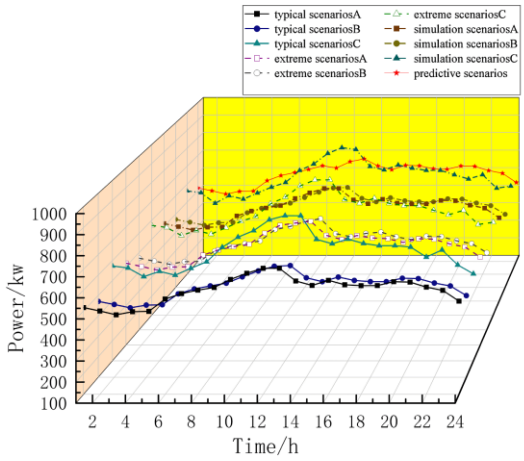

Figure 7. Normal load of the hybrid and simulation scenarios.

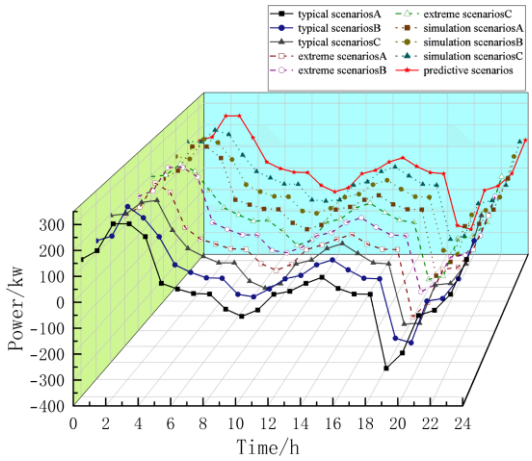

Figure 8. EV power output of the hybrid and simulation scenarios.

As shown in Figures 6–8, three simulation scenarios are selected: simulation scenario A, simulation scenario B, and simulation scenario C.

The simulation results are shown in Figures 9–13. As shown in Figure 9, during the periods 1:00–7:00 and 20:00–24:00, PV generation is unavailable, and the day-ahead electricity price is lower than the generation cost of the micro gas turbine. Therefore, the micro gas turbine operates at a lower power during these two periods. From 8:00 to 23:00, it runs at the maximum power to improve the economy by selling more power to the main grid (or reducing purchases).

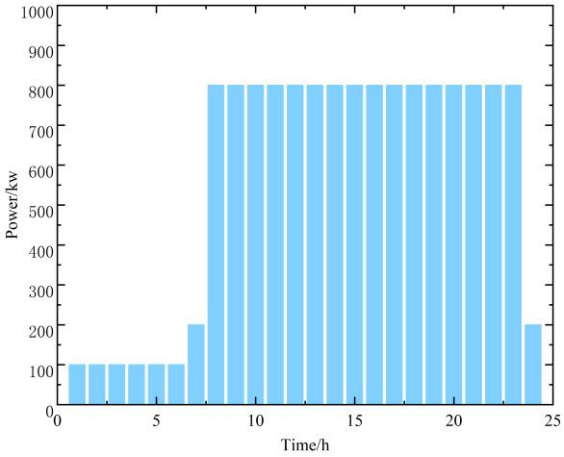

Figure 9. Power output of the micro gas turbine.

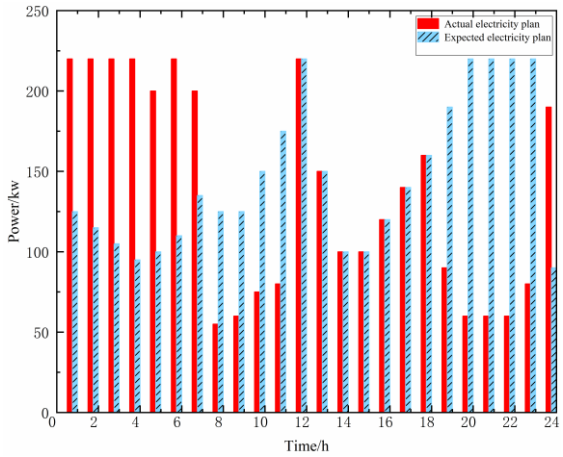

Figure 10. Expected/actual electricity plan of the demand response load.

As shown in Figure 10, the actual electricity plan is lower than expected during peak periods (8:00–11:00 and 19:00–23:00). During off-peak periods (1:00–7:00 and 24:00), the actual electricity plan exceeds the expected. By shifting deferrable loads from peak to off-peak periods, this strategy effectively achieves peak shaving and valley filling and significantly reduces the overall operating cost of the microgrid.

Figure 11 shows the power output of the energy storage system. A positive value indicates

discharge power, and a negative value indicates charge power. Under the guidance of time-of-use electricity price mechanism, the energy storage system is charged to store power during the periods of low electricity price (1:00–3:00 and 24:00). Similarly, the energy storage system is discharged during periods of high electricity price (9:00–10:00 and 22:00–23:00). The energy storage system effectively shaves peaks and fills valleys and significantly improves the economy of the microgrid.

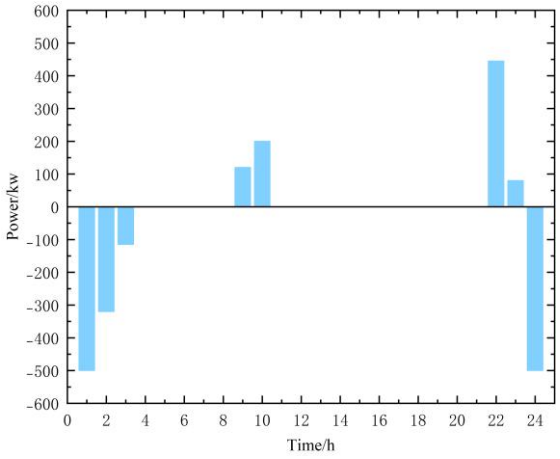

Figure 11. Power output of the energy storage system.

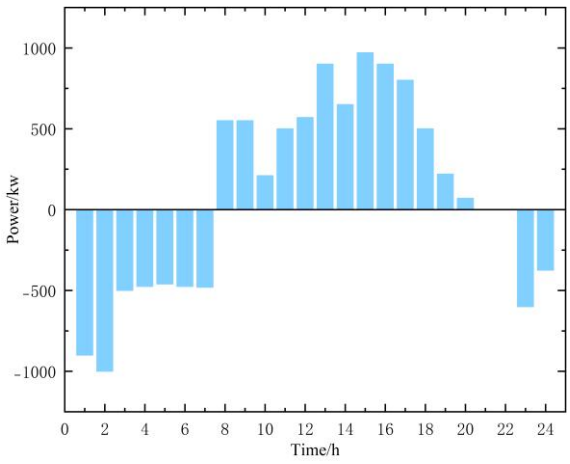

Figure 12. Power interaction of the microgrid.

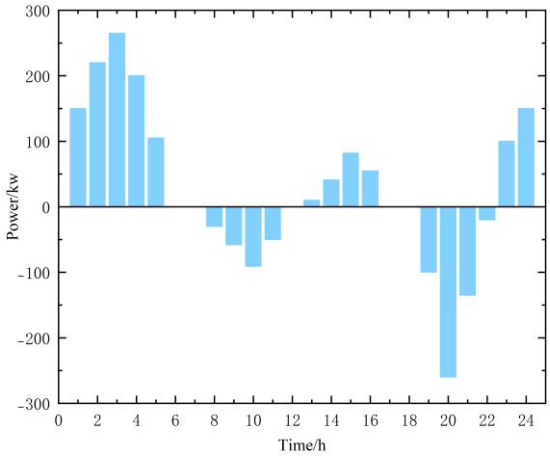

Figure 13. Charging and discharging power of EVs.

Figure 12 shows the microgrid's power interaction with the main grid, where a negative value indicates power purchase and a positive value indicates power sale. During the low-price valley periods (1:00–7:00, 24:00), the system primarily purchases electricity from the main grid to maintain balance, which is more economical than operating the gas turbine. Conversely, during the high-price peak periods (9:00–11:00, 17:00–21:00), the gas turbine operates at maximum output to sell excess electricity to the main grid, thereby enhancing the microgrid's economic return.

Figure 13 shows the power output of EVs. During the evening peak load periods 19:00–22:00,

plenty of EVs connect to the microgrid and participate in concentrated V2G discharging, effectively reducing the peak load. For the low-price valley periods (1:00–7:00, 23:00–24:00), charging is scheduled to meet the next day's travel needs at a lower cost. During daytime hours (7:00–17:00), even short-stay EVs participate in orderly dispatch. EVs are scheduled to discharge during high-price periods (7:00–11:00) and charge during lower-price periods (12:00–15:00). This strategy of charging during low-price periods and discharging during high-price periods effectively achieves peak shaving and valley filling while leveraging the time-of-use electricity price mechanism to enhance microgrid's economics.

Reference [17] designed a traditional two-stage robust optimization for EV-containing microgrids, which optimized the performance corresponding to the worst scenario (labeled as "Algorithm Ref-[17]" for ease of citation). Reference [21] designed a microgrid scheduling optimization based on the expected scenario, which can achieve the goal of "optimal for the expected scenario and feasible for worst scenario".

Note that the scheme in Reference [21] does not consider EVs. In order to make it possible to compare that with the proposed HSEV-RO algorithm, it is necessary to appropriately modify it by introducing EVs; the modified scheme is labeled as "Algorithm M-Ref-[21]". The comparison of economic performance between the HSEV-RO algorithm, "Ref-[17]" and "Algorithm M-Ref-[21]" is made here, and the results are shown in Table 2.

Table 2. Performance comparison of different algorithms.

Simulation scenarios	Methods	Day-ahead plan cost/CNY	Intraday adjustment cost/CNY	Total costs/CNY	Total cost reduction rate
Scenario A	Algorithm Ref-[17]	5683.5	1180.8	6864.3	-
	Algorithm M-Ref-[21]	5408.2	1263.6	6671.8	2.8%
	HSEV-RO	5531.4	1012.1	6543.5	4.6%
Scenario B	Algorithm Ref-[17]	5683.5	1258.4	6941.9	-
	Algorithm M-Ref-[21]	5408.2	1086.9	6495.1	6.4%
	HSEV-RO	5531.4	983.7	6470.1	6.8%
Scenario C	Algorithm Ref-[17]	5683.5	1686.9	7370.4	-
	Algorithm M-Ref-[21]	5408.2	2062.3	7470.5	-1.3%
	HSEV-RO	5531.4	1598.1	7129.5	3.2%

Table 2 reveals that the Algorithm Ref-[17] method results in the highest day-ahead cost due to its worst-case optimization, whereas Algorithm M-Ref-[21] achieves the lowest cost by targeting expected scenarios. Compared to Algorithm Ref-[17] and Algorithm M-Ref-[21], HSEV-RO takes into account the performance corresponding to multiple scenarios and achieves an intermediate day-ahead cost. For scenarios A, B, and C, the Algorithm Ref-[17] method achieved the highest intraday adjustment cost, while the HSEV-RO method achieved optimal intraday adjustment cost. In addition, for scenario A, the total cost of Algorithm M-Ref-[21] was reduced by 2.8% compared to Algorithm Ref-[17], and the total cost of HSEV-RO was further reduced to 4.6%. For scenario B, the total cost of Algorithm M-Ref-[21] decreased by 6.4% compared to Algorithm Ref-[17], while the total cost of HSEV-RO further decreased to 6.8%. For scenario C, the total cost of Algorithm M-Ref-[21] increased by 1.3% compared to Algorithm Ref-[17], while the total cost of HSEV-RO further decreased to 3.2%. In summary, for scenarios A, B, and C, the HSEV-RO method achieved both the optimal intraday

adjustment cost and the optimal total operating cost, thereby effectively enhancing the overall economic efficiency of the microgrid.

Since the HSEV-RO algorithm carries out multiple-scenario performance optimization over the entire hybrid scenario set in the day-ahead stage, it can yield a much better scheduling plan that aligns more closely with actual intraday scenarios. By transferring the optimized solution from the day-ahead stage, which better aligns with intraday scenarios, to the intraday scheduling phase, the coordination between day-ahead and intraday scheduling is significantly enhanced. This approach minimizes the intraday adjustment cost and total operating cost, thereby effectively improving the overall economic efficiency of microgrid.

The proposed HSEV-RO algorithm is built upon a centralized optimization framework, assuming a reliable and delay-free internal communication network within the microgrid. However, in practical engineering applications, communication delays, data packet loss, or network failures may lead to outdated status information or inaccurate execution of commands, which can affect real-time scheduling performance. Also, event-triggered or resilient distributed control strategies can be adopted to reduce dependence on high-performance communication and enhance the algorithm's practical applicability.

6. Conclusions

Based on hybrid-scenario performance, this study proposes a robust optimal scheduling algorithm for an electric vehicle-integrated microgrid, addressing uncertainties of PV, load, and EV charging/discharging scenarios. Through simulation experiments and analysis, the following conclusions are obtained:

(1) A hybrid scenario set including typical scenarios, extreme scenarios, and expected scenarios is constructed by applying Fuzzy C-Means clustering to historical data. Furthermore, typical scenarios, extreme scenarios, and expected scenarios are designated as the clustering center of the scenario set, and each historical scenario is reassigned to the closest clustering center through secondary clustering. Thus, the probability of the above clustering center is generated.

(2) A robust optimization method for the microgrid is designed by optimizing performance over the hybrid scenario set. The comprehensive coverage of the hybrid scenario set enables the generation of a day-ahead optimal solution with enhanced alignment to actual intraday conditions of renewables, load, and EVs. As a result, it reduces the adjustment cost during intraday scheduling stage, ultimately improving the microgrid's robustness and economic performance.

(3) Using a Monte Carlo simulation, it constructs the uncertainty intervals for EV power. Synthesizing performance optimization of the hybrid scenario set and robust testing, it achieves the goal of "optimal for hybrid scenarios and feasible for any scenario", improving the economic performance and robustness of the microgrid.

(4) Current charging patterns of electric vehicle owners, establishment of autonomous decision-making models, and user behavior patterns are hot topics of discussion [22–25]. This study focuses on a simplified model of EV behavioral uncertainty, without explicitly accounting for the uncertainty in users' response to incentives. Future work will address these aspects by incorporating travel demands and user response variability, integrating behavioral modeling and game theory to enhance practicality.

Use of AI tools declaration

The authors declare they have not used Artificial Intelligence (AI) tools in the creation of this article.

Acknowledgments

This research is supported by National Natural Science Foundation of China (61573239) and Open Project Program of Key Laboratory of System Control and Information Processing, Ministry of Education, Shanghai (Scip201509).

Conflict of interest

The authors declare no conflicts of interest.

Author contributions

Guanglin Song: Conceptualization, Methodology, Formal analysis, Investigation, Writing—original draft. Pengyuan Zheng: Supervision—review and editing. Chen Wei: Conceptualization—review and editing. Jiabin Xue Conceptualization—review and editing. Dong Wang: Formal Analysis.

References

1. Sadeghian O, Oshnoei A, Mohammadi-ivatloo B, et al. (2022) A comprehensive review on electric vehicles smart charging: Solutions, strategies, technologies, and challenges. *J Energy Storage* 54: 105241. https://doi.org/10.1016/j.est.2022.105241
2. Tabatabaee S, Mortazavi SS, Niknam T (2017) Stochastic scheduling of local distribution systems considering high penetration of plug-in electric vehicles and renewable energy sources. *Energy* 121: 480–490. https://doi.org/10.1016/j.energy.2016.12.115
3. Wu M, Zhang N, Liang Y, et al. (2024) Research and development of microgrid technology in the context of new type power system. *New Power Syst* 2: 251–271. Available from: http://ntps.epri.sgcc.com.cn/CN/10.20121/j.2097-2784.ntps.240049.
4. Kempton W, Tomic J (2005) Vehicle-to-grid power fundamentals: Calculating capacity and net revenue. *J Power Sources* 144: 268–279. https://doi.org/10.1016/j.jpowsour.2004.12.025
5. Zhang M, Chen J (2014) The energy management and optimized operation of electric vehicles based on microgrid. *IEEE Trans Power Delivery* 29: 1427–1435. https://doi.org/10.1109/TPWRD.2014.2303492
6. Chang S, Niu Y, Jia T (2021) Coordinate scheduling of electric vehicles in charging stations supported by microgrids. *Electr Power Syst Res* 199: 107418. https://doi.org/10.1016/j.epsr.2021.107418
7. Bhowmick A, Badar AQH (2024) Bi-level optimization for energy management of networked microgrid. *2024 IEEE 4th International Conference on Sustainable Energy and Future Electric Transportation (SEFET)*, 1−6. https://doi.org/10.1109/SEFET61574.2024.10718199
8. Liu Y, Guo L, Wang C (2018) Economic dispatch of microgrid based on two stage robust optimization. *Proc CSEE* 38: 4013–4022. https://doi.org/10.13334/j.0258-8013.pcsee.170500

9. Liang Z, Yin X, Chung CY, et al. (2025) Managing massive RES integration in hybrid microgrids: A data-driven quad-level approach with adjustable conservativeness. *IEEE Trans Ind Inf* 21: 7698–7709. https://doi.org/10.1109/TII.2025.3575133
10. Liang Z, Chung CY, Wang Q, et al. (2025) Fortifying renewable-dominant hybrid microgrids: A Bi-Directional converter-based interconnection planning approach. *Engineering* 51: 130–143. https://doi.org/10.1016/j.eng.2025.02.020
11. Ratanakuakangwan S, Morita H (2021) Hybrid stochastic robust optimization and robust optimization for energy planning—A social impact-constrained case study. *Appl Energy* 298: 117258. https://doi.org/10.1016/j.apenergy.2021.117258
12. Dashti H, Cheng J, Krokhmal P, et al. (2022) Chance-constrained optimization-based solar microgrid design and dispatch for radial distribution networks. *Energy Syst* 13: 959–981. https://doi.org/10.1007/s12667-020-00418-4
13. Zandrazavi SF, Guzman CP, Tabares A, et al. (2022) Stochastic multi-objective optimal energy management of grid-connected unbalanced microgrids with renewable energy generation and plug-in electric vehicles. *Energy* 241: 122884. https://doi.org/10.1016/j.energy.2021.122884
14. Xie C, Yang X, Chen T, et al. (2024) A Low-carbon robust optimization scheduling model for microgrids considering electric vehicles. *2024 9th Asia Conference on Power and Electrical Engineering (ACPEE)*, 1603−1609. https://doi.org/10.1109/ACPEE60788.2024.10532602
15. Jiang L, Zhang Y, Xiao C, et al. (2022) Optimal scheduling of electric vehicle clusters considering uncertainty of user demand response. *2022 IEEE 6th Conference on Energy Internet and Energy System Integration (EI2)*, Chengdu, China, 2927–2930. https://doi.org/10.1109/EI256261.2022.10116605
16. Chen X, Zhai J, Jiang Y, et al. (2023) Decentralized coordination between active distribution network and multi-microgrids through a fast decentralized adjustable robust operation framework. *Sustainable Energy Grids Networks* 34: 101068. https://doi.org/10.1016/j.segan.2023.101068
17. Shao S, Ma X, Yuan W, et al. (2023) Robust optimal dispatching method for uncertain microgrid including electric vehicles. *J Electr Eng* 18: 201−209. https://doi.org/10.11985/2023.02.020
18. Chen P, Liu Y, Yuan C, et al. (2025) Strategy for enhancing the available capacity of distribution networks considering electric vehicle charging modes. *Power Syst Technol* 49: 177−186. https://doi.org/10.13335/j.1000-3673.pst.2023.2236
19. Sujil A, Kumar R, Bansal RC (2025) FCM Clustering-ANFIS-based PV and wind generation forecasting agent for energy management in a smart microgrid. *J Eng* 18: 4852−4857. https://doi.org/10.1049/joe.2018.9323
20. Pugazhenthi A, Kumar LS (2020) Selection of optimal number of clusters and centroids for K-means and Fuzzy C-means clustering: A review. *2020 5th International Conference on Computing, Communication and Security (ICCCS),* Patna, India, 1−4. https://doi.org/10.1109/ICCCS49678.2020.9276978
21. Sang B, Zhang T, Liu Y, et al. (2020) Two-stage robust optimal scheduling of grid-connected microgrid under expected scenarios. *IET Gener Transm Distrib* 14: 6161–6173. https://doi.org/10.1049/iet-gtd.2020.1113
22. Fan P, Li S, Bu S, et al. (2025) Resilient power systems against wildfire risks: Towards a human-centric and secure future. *CSEE J Power Energy Syst* 11: 2553–2575. https://doi.org/10.17775/CSEEJPES.2025.02920

23. Fan P, Yang J, Ke S, et al. (2024) A multi-layer intelligent control strategy for multi-regional power system with electric vehicles: A deep reinforcement learning approach. *J Energy Storage* 103: 114381. https://doi.org/10.1016/j.est.2024.114381
24. Yeo S, Lee DJ (2021) Selecting the optimal charging strategy of electric vehicles using simulation based on users' behavior pattern data. *IEEE Access* 9: 89823–89833. https://doi.org/10.1109/ACCESS.2021.3090437
25. Wu F, Yang J, Li B (2024) Uncertain scheduling potential of charging stations under multi-attribute uncertain charging decisions of electric vehicles. *Appl Energy* 347: 12406. https://doi.org/10.1016/j.apenergy.2024.124036

AIMS Press